

Tuning Interfacial Spins in Antiferromagnetic–Ferromagnetic–Heavy-Metal Heterostructures via Spin-Orbit Torque

X. H. Liu^{1,2,*}, K. W. Edmonds,³ Z. P. Zhou^{1,2}, and K. Y. Wang^{1,2,4,5,†}

¹State Key Laboratory for Superlattices and Microstructures, Institute of Semiconductors, Chinese Academy of Sciences, Beijing 100083, China

²Center of Materials Science and Optoelectronics Engineering, University of Chinese Academy of Sciences, Beijing 100049, China

³School of Physics and Astronomy, University of Nottingham, Nottingham NG7 2RD, United Kingdom

⁴Beijing Academy of Quantum Information Sciences, Beijing 100193, China

⁵Center for Excellence in Topological Quantum Computation, University of Chinese Academy of Science, Beijing 100049, China



(Received 24 September 2019; revised manuscript received 30 November 2019; published 29 January 2020)

Antiferromagnets are outstanding candidates for the next generation of spintronic applications, with great potential for downscaling and decreasing power consumption. Recently, the manipulation of bulk properties of antiferromagnets has been realized by several different approaches. However, the interfacial spin order of antiferromagnets is an important integral part of spintronic devices, and thus, the successful control of interfacial antiferromagnetic spins is urgently desired. Here, we report the high controllability of interfacial spins in antiferromagnetic–ferromagnetic–heavy-metal heterostructure devices using spin-orbit torque (SOT) assisted by perpendicular or longitudinal magnetic fields. Switching of the interfacial spins from one direction to another through multiple intermediate states is demonstrated. The field-free SOT-induced reorientation of antiferromagnetic interfacial spins is also observed, which we attribute to the effective built-in out-of-plane field due to unequal upward and downward interfacial spin populations. Our work provides a precise way to modulate the interfacial spins at an antiferromagnet/ferromagnet interface via SOT, which will greatly promote innovative designs for next-generation spintronic devices.

DOI: 10.1103/PhysRevApplied.13.014059

I. INTRODUCTION

Antiferromagnets have numerous advantageous properties for future spintronics applications: robustness against external field, no stray fields, and ultrafast spin dynamics [1,2]. In particular, the recent discovery of electrical switching of an antiferromagnet by spin-orbit torque (SOT) shows that antiferromagnets can be electrically manipulated in similar ways to their ferromagnetic (FM) counterparts [3]; this is stimulating considerable research into antiferromagnetic (AFM) spintronics [4–8]. To date, most work has focused on electrical manipulation of bulk properties of AFM materials [3–12]. Conversely, from the point of view of expanding the functionality and design flexibility in AFM spintronic devices, developing methods to tune the interfacial properties of AFM materials through SOT is a vitally significant issue.

Exchange bias (EB) refers to a shift in the hysteresis loop along the magnetic field axis due to interfacial

exchange coupling between adjacent FM-AFM layers. This phenomenon has been extensively studied because of its technological importance, for example, in read heads for magnetic storage or spin valves [13,14]. Moreover, it offers a unique tool to directly probe the AFM interfacial spin states and interfacial exchange coupling. EB can be utilized to exert an internal effective field in a heavy-metal (HM)-FM system to obtain deterministic SOT switching of a perpendicular magnetic anisotropy (PMA) magnetization [15–20]. In the past decade, the electrical control of EB in FM-AFM heterostructures has been demonstrated using multiferroic AFM insulators YMnO₃, BiFeO₃, or Cr₂O₃ [21–23]. However, this effective electrical control faces a big challenge for metallic AFM materials, such as Ir-Mn or Pt-Mn. Very recently, Lin *et al.* discovered the concurrent switching of FM magnetization and EB by SOT in a HM-FM-AFM trilayer system [24].

Here, we report the high tunability of AFM interfacial spins by SOT combined with perpendicular or longitudinal magnetic fields in a HM-FM-AFM system. We can effectively switch the AFM interfacial spins between multiple different states, using different combinations of pulsed

*xionghualiu@semi.ac.cn

†kywang@semi.ac.cn

electrical currents and magnetic fields. Moreover, an irreversible SOT-induced reorientation of AFM interfacial spins in zero magnetic field is demonstrated. The realization of AFM interfacial multistate spin switching via SOT, with or even without external fields, will enlarge the designability of AFM spintronics.

II. EXPERIMENT

The stack structures of Ta(0.6)/Pt(3)/Co(0.8)/Ir₂₅Mn₇₅(*t*)/Ta(2) (thicknesses in nm) with *t* = 5, 6, 7, and 8 nm are deposited on thermally oxidized Si substrates by magnetron sputtering at room temperature. The bottom and top Ta layers are used for adhesion and capping layers, respectively. The base pressure is less than 1×10^{-8} Torr before deposition, and the pressure of the sputtering chamber is 0.8 mTorr during deposition. No magnetic field is applied during sputtering. The deposition rates for Ta, Pt, Co, and Ir₂₅Mn₇₅ films are controlled to be approximately 0.016, 0.025, 0.012, and 0.015 nm/s, respectively. Subsequently, the samples are patterned into Hall bar devices with channel widths of 10 μ m by photolithography and Ar-ion etching. For field-annealing treatments, the fabricated devices are annealed at 250 °C for 30 min at a base vacuum of 1×10^{-7} Torr under an out-of-plane [along the *z* direction in Fig. 1(b)] magnetic field of 0.7 T, then are field-cooled to room temperature, by using oven for magnetic-field annealing (F800-35, East Changning Technologies, China). The Kerr characterization of

magnetization hysteresis is achieved using a NanoMoke3 magneto-optical Kerr magnetometer. The anomalous Hall effect measurements are carried out at room temperature with a Keithley 2602 instrument as the source meter and a Keithley 2182 instrument as the nanovoltage meter.

III. ANTFERROMAGNETIC LAYER THICKNESS DEPENDENCE

Experiments are performed on Ta(0.6)/Pt(3)/Co(0.8)/Ir₂₅Mn₇₅(*t*_{Ir-Mn})/Ta(2) (in nm) stacks, with *t*_{Ir-Mn} = 5, 6, 7, and 8 nm, as schematically illustrated in Fig. 1(a). Figure 1(b) presents an optical micrograph of a typical Hall bar, along with the definition of the coordinate system. The anomalous Hall effect resistance (*R*_H), as a function of the out-of-plane field (*B*_z), for as-grown samples (i.e., without field annealing) with *t*_{Ir-Mn} = 5, 6, 7, and 8 nm, before applying pulsed currents, are exhibited in Figs. 1(c)–1(f). A square hysteresis loop is found for samples with *t*_{Ir-Mn} = 5 and 6 nm, with much larger coercivity for *t*_{Ir-Mn} = 6 nm, while no EB is observed for either sample. Similar results are also observed elsewhere [24]. Two-step switching behavior is observed for samples with *t*_{Ir-Mn} = 7 and 8 nm, with stronger out-of-plane pinning observed for *t*_{Ir-Mn} = 8 nm [Fig. 1(e) and 1(f)].

The as-grown Hall bar samples are then subjected to a sequence of current pulses along the *x* direction, of varying amplitude *I*_p and fixed width of 50 ms, in a longitudinal applied field of *B*_x = 0.1 T [Fig. 1(g)]. Through the spin

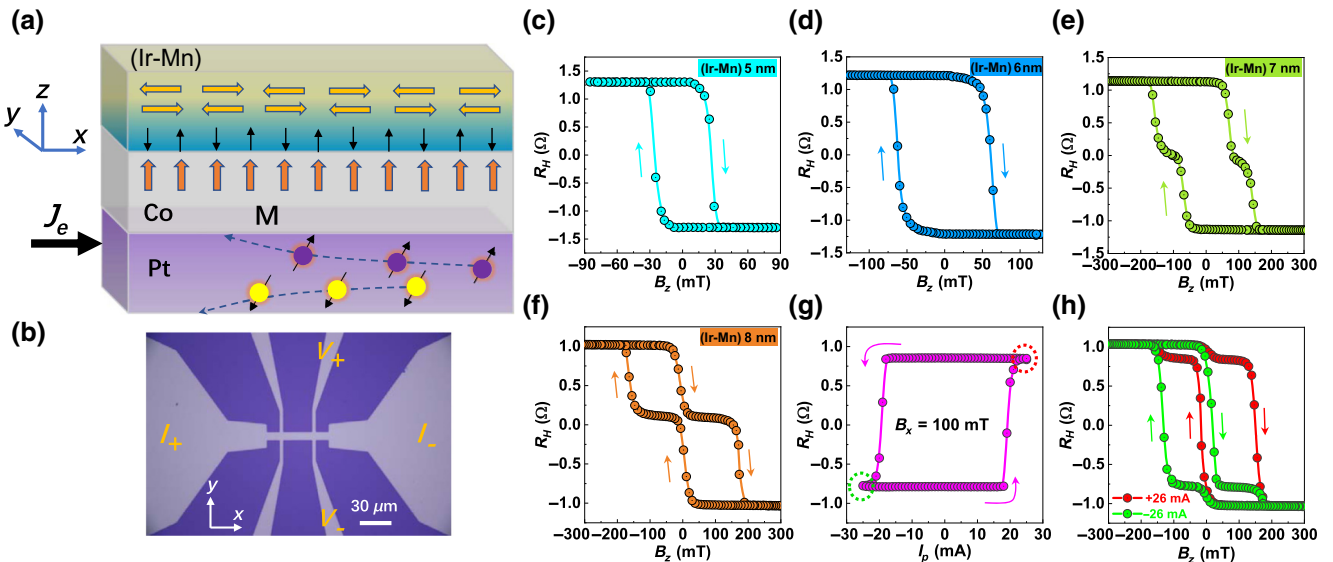


FIG. 1. Sample structure and magnetic properties. (a) Schematic of the studied HM-FM-AFM trilayer system with a definition of the *x*-*y*-*z* coordinates. (b) Optical micrograph of the fabricated Hall device and measurement scheme. (c)–(f) Anomalous Hall resistance, *R*_H, versus perpendicular magnetic field, *B*_z, curves for as-grown samples with *t*_{Ir-Mn} = 5, 6, 7, and 8 nm, respectively, before applying pulsed currents. The magnetic properties vary with *t*_{Ir-Mn}, with two-step behavior observed for samples with *t*_{Ir-Mn} = 7 and 8 nm. (g) *R*_H versus current pulse amplitude, *I*_p, under in-plane field *B*_x = 0.1 T for the sample with *t*_{Ir-Mn} = 8 nm, showing current-induced switching of the FM layer. (h) *R*_H versus *B*_z curves measured after the applied current pulses, demonstrating switching of the AFM interfacial spins.

Hall effect (SHE), a charge current in the $\pm x$ direction should produce a spin polarization along the $\pm y$ direction for the positive spin Hall angle of Pt [25]. The resulting spin current can switch the magnetization of PMA Co between the $\pm z$ directions, provided that both the current density and B_x are large enough. Moreover, the absorption of transverse spin currents is found to vary with the FM thickness, with a characteristic saturation length of 1.2 nm [26]. Thus, in our devices, not only can the 0.8 nm thick Co layer, but also the AFM interfacial spins, be directly affected by SOT. Figure 1(g) shows the measured R_H after each current pulse for the sample with $t_{\text{Ir-Mn}} = 8 \text{ nm}$, showing a square loop consistent with deterministic switching of the FM perpendicular magnetization.

The R_H versus B_z loops, obtained after the application of current pulses $I_p = \pm 26 \text{ mA}$ in $B_x = 0.1 \text{ T}$, are shown in Fig. 1(h). In this process, first, we set $B_x = 0.1 \text{ T}$ and then apply a single pulse $I_p = 26 \text{ mA}$; after that, we set $B_x = 0$ and $I_p = 0$ and measure the R_H versus B_z loop. The R_H versus B_z loop for $I_p = -26 \text{ mA}$ under $B_x = 0.1 \text{ T}$ is obtained by using the same process. The main part of the loop displays negative EB for a single pulse $I_p = 26 \text{ mA}$ (red) and positive EB for a single pulse -26 mA (green). The opposite behavior of R_H versus B_z and R_H versus I_p curves are observed for $B_x = -0.1 \text{ T}$ (see Fig. S1 within the Supplemental Material [27]). The SOT-induced EB switching is also found for $t_{\text{Ir-Mn}} = 7 \text{ nm}$, but not for $t_{\text{Ir-Mn}} = 5 \text{ and } 6 \text{ nm}$ (see Fig. S2 within the Supplemental Material [27]).

Two-step hysteresis loops, similar to the one shown in Fig. 1(f), are commonly observed in as-deposited or zero-field-cooled FM-AFM bilayers. They are related to the occurrence of a bidomain state, in which the two domain populations are oppositely exchange biased due to opposite orientations of the uncompensated AFM spins at the FM-AFM interface [28,29]. The switching behavior observed in Fig. 1(h) is consistent with a change in the populations of the two domain types, due to a reorientation of interfacial AFM spins during the current pulse.

The effect of the Joule heating on the exchange bias reversal must be considered [20]. To estimate the temperature rise due to Joule heating, the resistance of the sample is measured during the current pulse for the sample with $t_{\text{Ir-Mn}} = 7 \text{ nm}$. By comparing this to the measured temperature dependence of resistance, a temperature rise of around 35 K is estimated for a 26 mA 50 ms current pulse (see Fig. S3 within the Supplemental Material [27]). In contrast, the blocking temperature for the $t_{\text{Ir-Mn}} = 7 \text{ nm}$ sample, defined as the temperature where the EB disappears, is around 450 K (see Fig. S4 within the Supplemental Material [27]). Therefore, we rule out a significant role of Joule heating in the observed switching. Furthermore, Ir-Mn alloys are reported to have a spin Hall angle with the same sign as that of Pt, but with a smaller value [30,31]. From the SOT switching data, the dominant contribution is from

the bottom Pt layer; moreover, the resistivity of Ir-Mn is about one order bigger than that of Pt, so that the current density in the Pt layer is about 10 times larger. Thus, the spin current contribution from Ir-Mn can be ignored in this system, similar to the work in Ref. [24].

We attribute the observed switching to the direct effect of the current-induced SOT on the uncompensated AFM spins at the FM-AFM interface. The spin current due to the SHE in the Pt layer induces a dampinglike torque, $\mathbf{m} \times (\boldsymbol{\sigma} \times \mathbf{m})$ (along the y direction), and a fieldlike torque, $\mathbf{m} \times \boldsymbol{\sigma}$ (along the x direction), where m is the interfacial spin moment and σ is the spin polarization of the spin current [32–38]. When the interfacial spins are deflected from the z direction due to SOT, switching into the direction of the FM layer magnetization will occur. The latter is determined by the relative alignments of I_p and B_x (see Fig. S1 within the Supplemental Material [27]).

IV. TUNING INTERFACIAL SPINS VIA SOT WITH LONGITUDINAL AND PERPENDICULAR FIELDS

Further investigations are focused on the tunability of AFM interfacial spins through SOT with the assistance of B_x or B_z . Figure 2 shows R_H versus B_z curves for the as-grown sample with $t_{\text{Ir-Mn}} = 8 \text{ nm}$ after applying current pulses under different external fields, together with schematics of the interfacial spin configurations (here, we only present the configurations under positive saturated B_z , all the spin moments of Co point upward). For the initial state, the observed two-step R_H versus B_z switching behavior shows approximately equal weighting of its upper and lower parts; this indicates no preference between upward and downward pinning directions for the interfacial spins [Fig. 2(a)]. We then investigate the effect of applying current pulses under different external magnetic field configurations, where the current pulse width is fixed at 50 ms and the magnitude of the current pulse (I_p) is fixed at 26 mA. The external magnetic field magnitude and direction during the current pulse is shown in the top panel of Fig. 2. After each treatment, the R_H versus B_z curve (as shown in the middle panel of Fig. 2) is measured. After a positive single current pulse of 26 mA under $B_x = 0.1 \text{ T}$, a negative EB is observed, with the two-step R_H versus B_z loop heavily weighted towards the lower part [Fig. 2(b)]. The opposite trend is found after applying $-I_p$ (-26 mA) under B_x (0.1 T) [Fig. 2(c)]. Both curves are exhibited in Fig. 1(h). Further increases of $|I_p|$ ($>26 \text{ mA}$) or B_x ($>0.1 \text{ T}$) do not further modify the R_H versus B_z loops, which indicates that the remaining oppositely aligned interfacial spins cannot be modified by SOT with the external field applied purely along x .

Applying I_p under $B_z = 0.25 \text{ T}$ results in a single-step R_H versus B_z loop with positive EB [Fig. 2(d)], which indicates a complete alignment of the interfacial spins in the direction of B_z . Subsequently applying $-I_p$ under

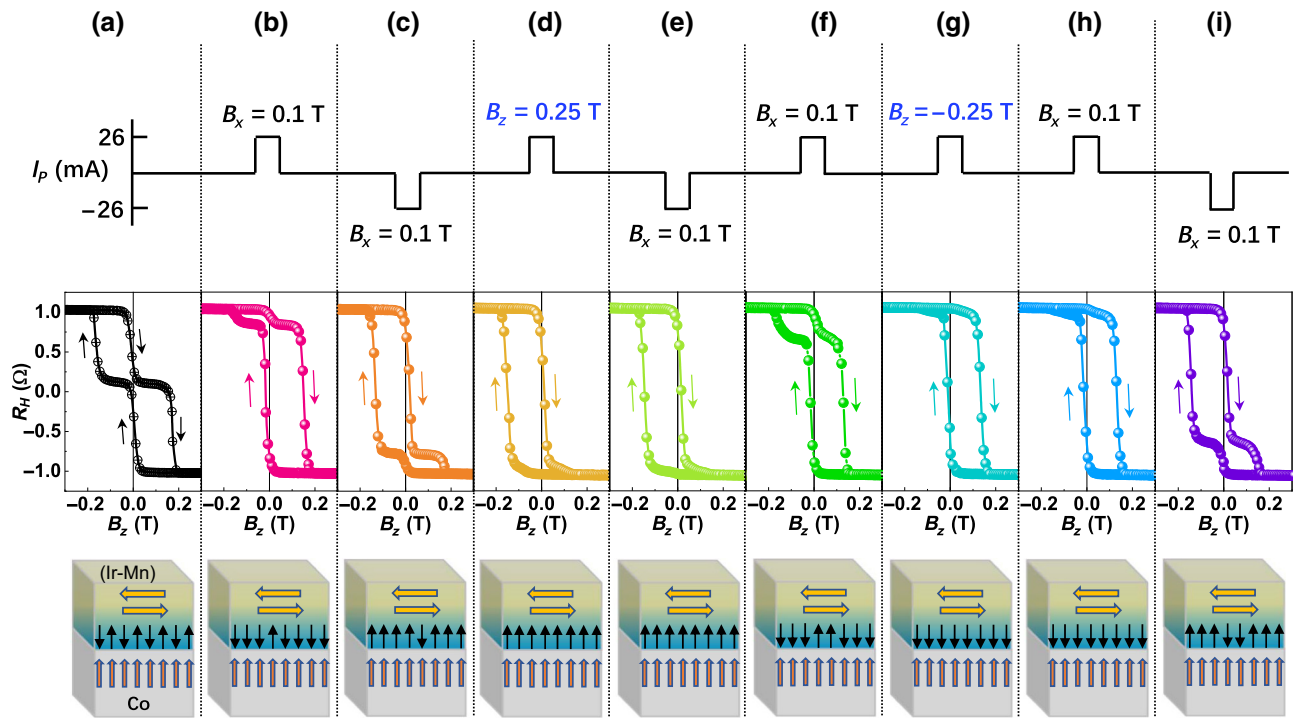


FIG. 2. AFM interfacial spins tuned by SOT. Sequences of current pulses with B_x or B_z applied to the as-grown sample with $t_{\text{Ir-Mn}} = 8 \text{ nm}$, R_H versus B_z curves, and schematics of the corresponding configurations of AFM and FM layers. (a) Initial state. (b) After applying $I_p = 26 \text{ mA}$ in $B_x = 0.1 \text{ T}$. (c) After applying $I_p = -26 \text{ mA}$ in $B_x = 0.1 \text{ T}$. (d) After applying $I_p = 26 \text{ mA}$ in $B_z = 0.25 \text{ T}$. (e) After applying $I_p = -26 \text{ mA}$ in $B_x = 0.1 \text{ T}$. (f) After applying $I_p = 26 \text{ mA}$ in $B_x = 0.1 \text{ T}$. (g) After applying $I_p = 26 \text{ mA}$ in $B_z = -0.25 \text{ T}$. (h) After applying $I_p = 26 \text{ mA}$ in $B_x = 0.1 \text{ T}$. (i) After applying $I_p = -26 \text{ mA}$ in $B_x = 0.1 \text{ T}$.

$B_x = 0.1 \text{ T}$ does not affect the loop [Fig. 2(e)], while applying $+I_p$ under $B_x = 0.1 \text{ T}$ results in a partial switch [Fig. 2(f)]. Similarly, applying I_p under $B_z = -0.25 \text{ T}$ results in a single-step loop with negative EB [Fig. 2(g)]. The opposite trend can then be seen in Figs. 2(h) and 2(i), compared with that in Figs. 2(e) and 2(f), respectively. These results indicate that switching between multiple states of the AFM interfacial spins can be achieved via SOT combined with external magnetic fields.

V. SYSTEMATIC VARIATION OF PULSE CURRENT AND MAGNETIC FIELDS

Next, we systematically investigate how pulse current intensity and the magnitude of the assisting magnetic fields affect the magnetic configuration of the HM-FM-AFM trilayer structure. As the R_H versus I_p curves show in Fig. 3(a) for the as-grown sample with $t_{\text{Ir-Mn}} = 8 \text{ nm}$, the height of the loop $\Delta R_H = R_H^+ - R_H^-$ gradually increases upon increasing the range of I_p under fixed $B_x = 0.1 \text{ T}$, saturating with $I_p \geq 22 \text{ mA}$. Correspondingly, the step in the R_H versus B_z loops gradually moves to higher R_H values [Fig. 3(b)]. The opposite direction of I_p under the same B_x induces the opposite shift of the magnetization step, as shown for the $I_p = -20 \text{ mA}$ loop in Fig. 3(b).

The shape of the R_H versus B_z loop can be further controlled via SOT with varying B_z , as shown in Fig. 3(c). Here, the initial state is set by applying $I_p = 22 \text{ mA}$ under $B_z = -0.2 \text{ T}$ to obtain a single-step loop. Subsequent pulses of $I_p = 22 \text{ mA}$ under different B_z from 1 to 200 mT result in a continuously adjustable R_H step height. The switched fraction, defined as the ratio of the switched R_H step height to the whole-loop height ($R_H^+ - R_H^-$), is plotted versus B_z in Fig. 3(d). Two distinct behaviors are observed: the switched fraction increases sharply to about 82% with B_z from 1 to 5 mT (region I), and then gradually increases to 100% with further increasing B_z (region II). The curve's slope for region I is about two orders of magnitude higher than that for region II. Significantly, the switched fraction of 82%, marked by the dashed line in Fig. 3(d) at the boundary between regions I and II, is close to that for $I_p \geq 22 \text{ mA}$ with longitudinal field, as seen in Fig. 3(b). Therefore, the SOT-induced switching under B_x is only effective up to the upper limit of region I.

To understand the reason for the formation of these two regions, it is necessary to consider the influence of the anti-ferromagnetic domain structure of the Ir-Mn bulk. This may result in the pinning of a part of the interfacial spins in directions deviating from z . The interfacial spins with effective spin moments along the in-plane direction cannot be changed to the perpendicular direction through SOT

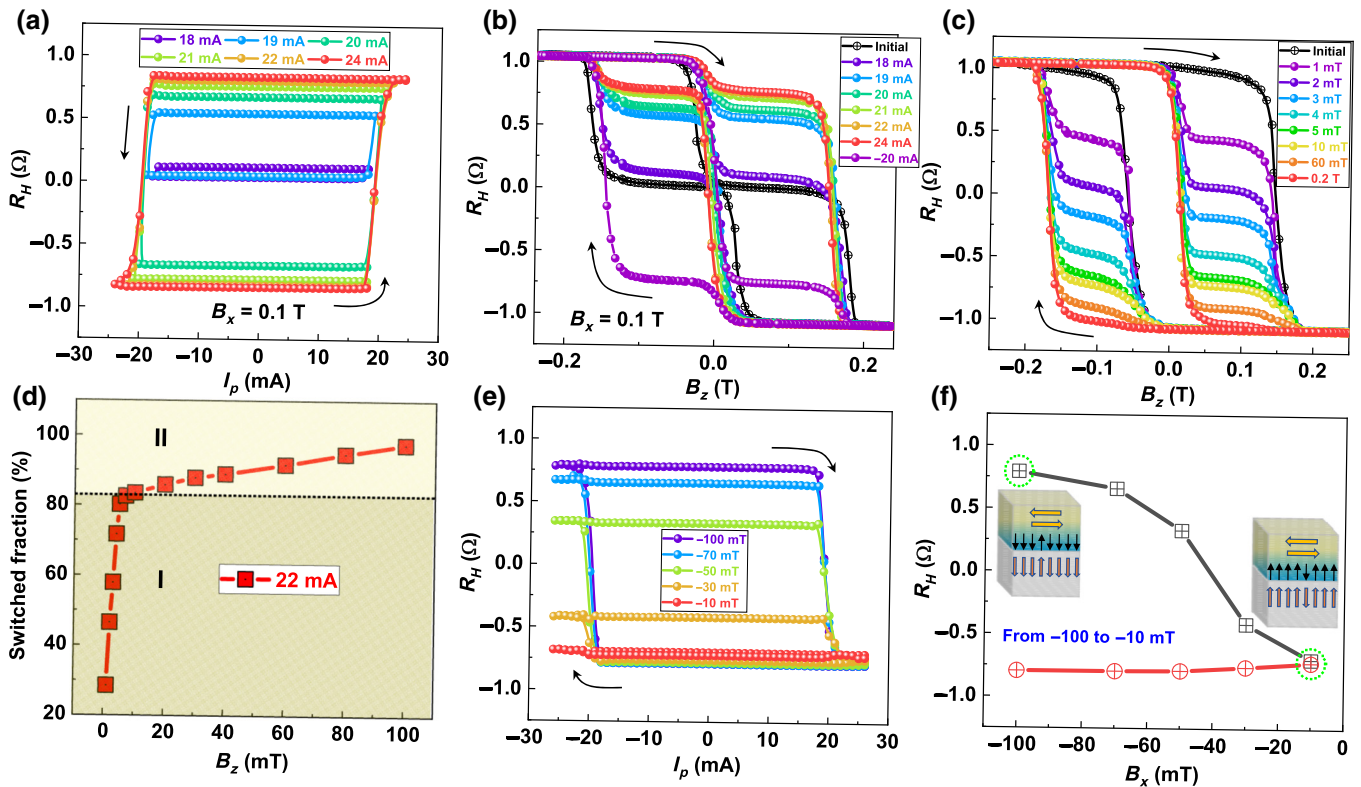


FIG. 3. Dependence on pulse current and magnetic field magnitudes. R_H versus B_z and R_H versus I_p curves for as-grown sample with $t_{\text{Ir-Mn}} = 8 \text{ nm}$. (a) R_H versus I_p curves with varying range of I_p and fixed $B_x = 0.1 \text{ T}$. (b) R_H versus B_z curves after varying I_p with fixed $B_x = 0.1 \text{ T}$. (c) R_H versus B_z curves after applying $I_p = 22 \text{ mA}$ under varying B_z , starting from an initial state set by applying $I_p = 22 \text{ mA}$ under $B_z = -0.2 \text{ T}$. (d) The switched fraction of interfacial spins obtained from the R_H versus B_z curves in (c), as a function of B_z . Two distinct regions are observed (indicated as I and II) separated by the dashed line at about 82%, and the slope for region I is around two orders of magnitude larger than that for region II. (e) R_H versus I_p curves for varying B_x . (f) The upper (R_H^+ , black) and lower (R_H^- , red) values of Hall resistance as a function of B_x obtained from (e). The schematic configurations of AFM interfacial spins and FM layers at the points marked by green circles are illustrated.

under B_x , resulting in a clear step in the R_H versus B_z curves in Fig. 3(b) for saturated I_p . Alternatively, the SOT under large B_z can flip all spins to the z direction with the assistance of a strong Zeeman interaction. Hence, the interfacial spins that remain unswitched under in-plane fields, corresponding to the boundary between regions I and II, can be related to in-plane pinning by Ir-Mn domains.

Furthermore, we find that positive and negative I_p have nearly the same effect on switching under B_z (see Fig. S5 within the Supplemental Material [27]). This is consistent with our interpretation of switching being due to the direct effect of the SOT on the AFM interfacial spins. A deflection of the interfacial spins from the perpendicular direction due to a current-induced SOT of either sign will enable their switching into the direction of B_z . Accordingly, a smaller SOT (due to a smaller pulsed current) requires a larger B_z to flip the interfacial spins, as shown in Fig. S6 within the Supplemental Material [27].

The effect of SOT with varying B_x on the interfacial spin configuration is also observed. As shown in Figs. 3(e) and 3(f), upon changing B_x from -100 to -10 mT , R_H

remains nearly constant, while R_H^+ is gradually reduced. Therefore, the SOT switching is gradually reduced with decreasing negative B_x . Similarly, the R_H versus I_p curves with varying B_x from 100 to 10 mT exhibit a constant R_H^+ and a gradual change of R_H^- (see Fig. S7 within the Supplemental Material [27]). However, after annealing the sample in a magnetic field along z , switching is found to be only weakly dependent on B_x in the range 10 – 100 mT (see Fig. S8 within the Supplemental Material [27]), because field annealing induces an out-of-plane effective field, which can assist the SOT switching. Therefore, switching can take place in quite small B_x in the field-annealed case.

VI. ZERO-FIELD SOT-INDUCED AFM INTERFACIAL SPIN REORIENTATION

We also observe a modification of the R_H versus B_z loop induced by current pulses in zero external field for the as-grown sample with $t_{\text{Ir-Mn}} = 8 \text{ nm}$ [Fig. 4(a)]. The initial state is set by applying $I_p = 22 \text{ mA}$ under $B_z = -0.2 \text{ T}$, and

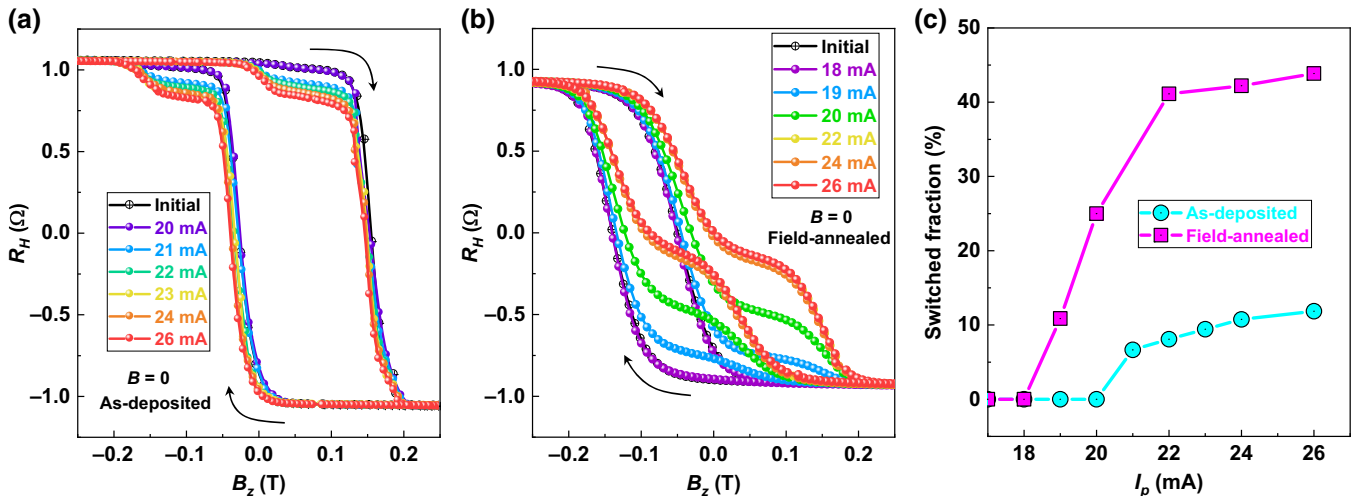


FIG. 4. SOT-induced variation under zero magnetic field. (a),(b) R_H versus B_z curves after different pulsed currents for $t_{\text{Ir-Mn}} = 8 \text{ nm}$ in zero field. For (a), the initial state is set by applying $I_p = 22 \text{ mA}$ under $B_z = -0.2 \text{ T}$ at room temperature. For (b), the initial state is set by annealing the sample at 250°C in a magnetic field $B_z = 0.7 \text{ T}$ and then field cooling to room temperature. (c) The switched fraction obtained from the R_H versus B_z curves in (a),(b), as a function of I_p for the as-deposited and field-annealed devices.

subsequent loops are obtained after applying I_p of varying magnitude under zero field. As shown in Fig. 4(a), after pulsing in zero field, the R_H versus B_z behavior transforms from a single-step loop, similar to that in Fig. 2(g) for the initial state, to a two-step loop, similar to that in Fig. 2(b). The effect is much more pronounced for the field-annealed sample [Fig. 4(b)]. Comparing the switched fractions versus I_p in Fig. 4(c), a smaller threshold I_p and a much larger switched fraction are observed for the field-annealed sample. The saturated state after zero-field SOT in Fig. 4(b) is close to the initial state of the as-grown device [see Fig. 2(a)], with nearly equal upward and downward parts of the loop.

In HM-FM systems with PMA, it is necessary to break the symmetry between up and down magnetization directions to generate deterministic switching using SOT. Typically, this is achieved by applying an in-plane magnetic field collinear with the electric current, but lateral asymmetry [34], tilted magnetic anisotropy [39], an antiferromagnetic layer [15], a polarized ferroelectric substrate [36], interlayer exchange coupling [16,40], interfacial spin-orbit interaction [41], or competing spin currents [42] are also introduced to achieve field-free deterministic switching. In our system, the field-free SOT-induced interfacial spin reorientation should be related to the inequivalent upward and downward domain populations, which produces an effective out-of-plane field ($B_{z,\text{eff}}$). It can be considered as a training effect, in which the built-in $B_{z,\text{eff}}$ assists the SOT to alter the interfacial spins from a metastable single-domain state to an equilibrium state, with incomplete alignment of the interfacial spins. As the net $B_{z,\text{eff}}$ is zero for the equilibrium state, the field-free effect is not reversible upon reversing the current, which is different from the field-free

SOT magnetization switching in Refs. [15,16,34,36,39–42]. Instead, it provides an efficient way to initialize the interfacial spins via SOT at zero field.

VII. DISCUSSIONS AND CONCLUSION

We demonstrate a high controllability of the spin states at the FM-AFM interface via SOT. Multistate switching is achieved using SOT in combination with external magnetic fields B_z or B_x , while field-free variation from the fully aligned state is also realized. Our work provides a very efficient scheme for tuning of the uncompensated antiferromagnetic interfacial spin states via SOT, which will expand the designability of spintronic devices. For instance, the SOT magnetic random access memory (MRAM) can potentially be realized by varying the FM-AFM interface via SOT, in contrast to the conventional design. Multiple resistance states, and thus, high density storage, may be achieved in this SOT MRAM cell. Furthermore, combination with conventional field annealing and the pulsed electrical currents approaches will open up more potential applications in spintronic devices. For example, if the EB is initially set along a preferred in-plane axis (x or y) by field annealing, the current pulses can induce EB in the perpendicular direction without disturbing the in-plane EB. For magnetic sensors containing many cells with different exchange-bias directions, the current pulse offers a convenient approach to tune the EB in different directions. In addition, the precise control of interfacial spins at a FM-AFM interface by SOT might result in a multistate perpendicular ferromagnet, which has potential application in a synaptic emulator for neuromorphic computing.

ACKNOWLEDGMENTS

This work is supported by the National Key R&D Program of China (Grant No. 2017YFB0405700), the NSFC (Grants No. 11474272 and No. 61774144), and the Chinese Academy of Sciences (Grants No. QYZDY-SSW-JSC020, No. XDB28000000, and No. XDPB12).

-
- [1] V. Baltz, A. Manchon, M. Tsoi, T. Moriyama, T. Ono, and Y. Tserkovnyak, Antiferromagnetic spintronics, *Rev. Mod. Phys.* **90**, 015005 (2018).
- [2] J. Zelezny, P. Wadley, K. Olejnik, A. Hoffmann, and H. Ohno, Spin transport and spin torque in antiferromagnetic devices, *Nat. Phys.* **14**, 220 (2018).
- [3] P. Wadley *et al.*, Electrical switching of an antiferromagnet, *Science* **351**, 587 (2016).
- [4] O. Gomonay, T. Jungwirth, and J. Sinova, High Antiferromagnetic Domain Wall Velocity Induced by Néel Spin-Orbit Torques, *Phys. Rev. Lett.* **117**, 017202 (2016).
- [5] T. Kosub, M. Kopte, R. Hühne, P. Appel, B. Shields, P. Maletinsky, R. Hübner, M. O. Liedke, J. Fassbender, O. G. Schmidt, and D. Makarov, Purely antiferromagnetic magnetoelectric random access memory, *Nat. Commun.* **8**, 13985 (2017).
- [6] K. Olejnik, T. Seifert, Z. Kaspar, V. Novak, P. Wadley, R. P. Campion, M. Baumgartner, P. Gambardella, P. Němec, J. Wunderlich, J. Sinova, P. Kužel, M. Müller, T. Kampfrath, and T. Jungwirth, Terahertz electrical writing speed in an antiferromagnetic memory, *Sci. Adv.* **4**, 3566 (2018).
- [7] R. Lebrun, A. Ross, S. A. Bender, A. Qaiumzadeh, L. Baldrati, J. Cramer, A. Brataas, R. A. Duine, and M. Klau, Tunable long-distance spin transport in a crystalline antiferromagnetic iron oxide, *Nature* **561**, 222 (2018).
- [8] X. Z. Chen, R. Zarzuela, J. Zhang, C. Song, X. F. Zhou, G. Y. Shi, F. Li, H. A. Zhou, W. J. Jiang, F. Pan, and Y. Tserkovnyak, Antidamping-Torque-Induced Switching in Biaxial Antiferromagnetic Insulators, *Phys. Rev. Lett.* **120**, 207204 (2018).
- [9] Z. Qiu, Z. Hou, J. Barker, K. Yamamoto, O. Gomonay, and E. Saitoh, Spin colossal magnetoresistance in an antiferromagnetic insulator, *Nat. Mater.* **17**, 577 (2018).
- [10] H. Yan *et al.*, A piezoelectric, strain-controlled antiferromagnetic memory insensitive to magnetic fields, *Nat. Nanotech.* **14**, 131 (2019).
- [11] B. G. Park, J. Wunderlich, X. Marti, V. Holy, Y. Kurosaki, M. Yamada, H. Yamamoto, A. Nishide, J. Hayakawa, H. Takahashi, A. B. Shick, and T. Jungwirth, A spin-valve-like magnetoresistance of an antiferromagnet-based tunnel junction, *Nature Mater.* **10**, 347 (2011).
- [12] X. Marti *et al.*, Room-temperature antiferromagnetic memory resistor, *Nature Mater.* **13**, 367 (2014)..
- [13] J. Nogues and I. K. Schuller, Exchange bias, *J. Magn. Magn. Mater.* **192**, 203 (1999).
- [14] X. H. Liu, W. Liu, Z. D. Zhang, and C. F. Chang, Mediating exchange bias by Verwey transition in CoO/Fe₃O₄ thin film, *J. App. Phys.* **123**, 083903 (2018).
- [15] S. Fukami, C. Zhang, S. DuttaGupta, A. Kurenkov, and H. Ohno, Magnetization switching by spin-orbit torque in an antiferromagnet-ferromagnet bilayer system, *Nat. Mater.* **15**, 535 (2016).
- [16] Y. C. Lau, D. Betto, K. Rode, J. M. D. Coey, and P. Stamenov, Spin-orbit torque switching without an external field using interlayer exchange coupling, *Nat. Nanotech.* **11**, 758 (2016).
- [17] A. van den Brink, G. Vermijs, A. Solignac, J. Koo, J. T. Kohlhepp, H. J. M. Swagten, and B. Koopmans, Field-free magnetization reversal by spin-Hall effect and exchange bias, *Nat. Commun.* **7**, 10854 (2016).
- [18] Y. Oh, S. C. Baek, Y. M. Kim, H. Y. Lee, K. Lee, C. Yang, E. Park, K. Lee, K. Kim, G. Go, J. Jeong, B. Min, H. Lee, K. Lee, and B. G. Park, Field-free switching of perpendicular magnetization through spin-orbit torque in antiferromagnet/ferromagnet/oxide structures, *Nat. Nanotech.* **11**, 878 (2016).
- [19] D. Wu, G. Yu, C. Chen, S. A. Razavi, Q. Shao, X. Li, B. Zhao, K. L. Wong, C. He, Z. Zhang, P. K. Amiri, and K. L. Wang, Spin-orbit torques in perpendicularly magnetized Ir₂₂Mn₇₈/Co₂₀Fe₆₀B₂₀/MgO multilayer, *Appl. Phys. Lett.* **109**, 222401 (2016).
- [20] S. A. Razavi, D. Wu, G. Yu, Y. Lau, K. L. Wong, W. Zhu, C. He, Z. Zhang, J. M. D. Coey, P. Stamenov, P. K. Amiri, and K. L. Wang, Joule Heating Effect on Field-Free Magnetization Switching by Spin-Orbit Torque in Exchange-Biased Systems, *Phys. Rev. Appl.* **7**, 024023 (2017).
- [21] V. Laukhin, V. Skumryev, X. Marti, D. Hrabovsky, F. Sánchez, M. V. García-Cuenca, C. Ferrater, M. Varela, U. Lüders, J. F. Bobo, and J. Fontcuberta, Electric-Field Control of Exchange Bias in Multiferroic Epitaxial Heterostructures, *Phys. Rev. Lett.* **97**, 227201 (2006).
- [22] S. M. Wu, S. A. Cybart, P. Yu, M. D. Rossell, J. X. Zhang, R. Ramesh, and R. C. Dynes, Reversible electric control of exchange bias in a multiferroic field-effect device, *Nat. Mater.* **9**, 756 (2010).
- [23] X. He, Y. Wang, N. Wu, A. N. Caruso, E. Vescovo, K. D. Belashchenko, P. A. Dowben, and C. Binek, Robust isothermal electric control of exchange bias at room temperature, *Nat. Mater.* **9**, 579 (2010).
- [24] P.-H. Lin, B.-Y. Yang, M.-H. Tsai, P.-C. Chen, K.-F. Huang, H.-H. Lin, and C.-H. Lai, Manipulating exchange bias by spin-orbit torque, *Nat. Mater.* **18**, 335 (2019).
- [25] Y. C. Li, K. W. Edmonds, X. H. Liu, H. Z. Zheng, and K. Y. Wang, Manipulation of magnetization by spin-orbit torque, *Adv. Quantum Technol.* **2**, 1800052 (2019).
- [26] A. Ghosh, S. Auffret, U. Ebels, and W. E. Bailey, Penetration Depth of Transverse Spin Current in Ultrathin Ferromagnets, *Phys. Rev. Lett.* **109**, 127202 (2012).
- [27] See the Supplemental Material at <http://link.aps.org/supplemental/10.1103/PhysRevApplied.13.014059> for R_H versus I_p and R_H versus B_z curves for as-grown samples with different thicknesses of Ir-Mn (Figs. S1 and S2); determination of the temperature increase due to Joule heating during the current pulse (Fig. S3) and the blocking temperature of Ir-Mn (Fig. S4); R_H versus B_z curves in the fully aligned state and after applying positive and pulsed currents (Fig. S5); switched fraction of interfacial spins determined from the step in R_H versus B_z curves, as a function of perpendicular field B_z for different pulsed currents (Fig. S6);

- R_H versus I_p curves and schematic configurations of AFM and FM layers at R_H^+ and R_H^- for the as-grown sample with $t_{\text{Ir-Mn}} = 8 \text{ nm}$, for varying B_x from 100 to 10 mT (Fig. S7); R_H versus I_p curves for the sample with $t_{\text{Ir-Mn}} = 8 \text{ nm}$ after field annealing with the field along z , for varying B_x from 100 to 10 mT applied during the pulse, and R_H^+ and R_H^- as a function of B_x (Fig. S8).
- [28] S. Brück, J. Sort, V. Baltz, S. Surinach, J. S. Munoz, B. Dieny, M. D. Baro, and J. Nogues, Exploiting length scales of exchange-bias systems to fully tailor double-shifted hysteresis loops, *Adv. Mater.* **17**, 2978 (2005).
 - [29] J. Y. Chen, N. Thiagarajah, H. J. Xu, and J. M. D. Coey, Perpendicular exchange bias effect in sputter-deposited CoFe/IrMn bilayers, *Appl. Phys. Lett.* **104**, 152405 (2014).
 - [30] J. Zhou, X. Wang, Y. Liu, J. Yu, H. Fu, L. Liu, S. Chen, J. Deng, W. Lin, X. Shu, H. Y. Yoong, T. Hong, M. Matsuda, P. Yang, S. Adams, B. Yan, X. Han, and J. Chen, Large spin-orbit torque efficiency enhanced by magnetic structure of collinear antiferromagnet IrMn, *Sci. Adv.* **5**, eaau6696 (2019).
 - [31] J. B. S. Mendes, R. O. Cunha, O. Alves Santos, P. R. T. Ribeiro, F. L. A. Machado, R. L. Rodríguez-Suárez, A. Azevedo, and S. M. Rezende, Large inverse spin Hall effect in the antiferromagnetic metal $\text{Ir}_{20}\text{Mn}_{80}$, *Phys. Rev. B* **89**, 140406(R) (2014).
 - [32] I. M. Miron, K. Garello, G. Gaudin, P. J. Zermatten, M. V. Costache, S. Auffret, S. Bandiera, B. Rodmacq, A. Schuhl, and P. Gambardella, Perpendicular switching of a single ferromagnetic layer induced by in-plane current injection, *Nature* **476**, 189 (2011).
 - [33] L. Liu, C. F. Pai, Y. Li, H. W. Tseng, D. C. Ralph, and R. A. Buhrman, Spin-torque switching with the giant spin hall effect of tantalum, *Science* **336**, 555 (2012).
 - [34] G. Yu, P. Upadhyaya, Y. Fan, J. G. Alzate, W. Jiang, K. L. Wong, S. Takei, S. A. Bender, L. Chang, Y. Jiang, M. Lang, J. Tang, Y. Wang, Y. Tserkovnyak, P. K. Amiri, and K. L. Wang, Switching of perpendicular magnetization by spin-orbit torques in the absence of external magnetic fields, *Nat. Nanotech.* **9**, 548 (2014).
 - [35] X. Qiu, W. Legrand, P. He, Y. Wu, J. Yu, R. Ramaswamy, A. Manchon, and H. Yang, Enhanced Spin-Orbit Torque via Modulation of Spin Current Absorption, *Phys. Rev. Lett.* **117**, 217206 (2016).
 - [36] K. Cai, M. Yang, H. Ju, S. Wang, Y. Ji, B. Li, K. W. Edmonds, Y. Sheng, B. Zhang, N. Zhang, S. Liu, H. Zheng, and K. Y. Wang, Electric field control of deterministic current-induced magnetization switching in a hybrid ferromagnetic /ferroelectric structure, *Nat. Mater.* **16**, 712 (2017).
 - [37] M. Yang, K. Cai, H. Ju, K. W. Edmonds, G. Yang, S. Liu, B. Li, B. Zhang, Y. Sheng, S. Wang, Y. Ji, and K. Y. Wang, Spin-orbit torque in Pt/CoNiCo/Pt symmetric devices, *Sci. Rep.* **6**, 20778 (2016).
 - [38] Y. Cao, A. W. Rushforth, Y. Sheng, H. Zheng, and K. Y. Wang, Tuning a binary ferromagnet into a multistate synapse with spin-orbit-torque-induced plasticity, *Adv. Funct. Mater.* **29**, 1808104 (2019).
 - [39] L. You, O. Lee, D. Bhowmik, D. Labanowski, J. Hong, J. Bokor, and S. Salahuddin, Switching of perpendicularly polarized nanomagnets with spin orbit torque without an external magnetic field by engineering a tilted anisotropy, *Proc. Natl. Acad. Sci. USA* **112**, 10310 (2015).
 - [40] Y. Sheng, K. W. Edmonds, X. Ma, H. Zheng, and K. Y. Wang, Adjustable current-induced magnetization switching utilizing interlayer exchange coupling, *Adv. Electron. Mater.* **4**, 1800224 (2018).
 - [41] S. C. Baek, V. P. Amin, Y. W. Oh, G. Go, S. J. Lee, G. H. Lee, K. J. Kim, M. D. Stiles, B. G. Park, and K. J. Lee, Spin currents and spin-orbit torques in ferromagnetic trilayers, *Nature Mater.* **17**, 509 (2018).
 - [42] Q. Ma, Y. Li, D. B. Gopman, Y. P. Kabanov, R. D. Schull, and C. L. Chien, Switching a Perpendicular Ferromagnetic Layer by Competing Spin Currents, *Phys. Rev. Lett.* **120**, 117703 (2018).